Förster resonance energy transfer, absorption and emission spectra in multichromophoric systems. I. Full cumulant expansions and system-bath entanglement

Jian Ma and Jianshu Cao

Citation: The Journal of Chemical Physics **142**, 094106 (2015); doi: 10.1063/1.4908599
View online: http://dx.doi.org/10.1063/1.4908599
View Table of Contents: http://scitation.aip.org/content/aip/journal/jcp/142/9?ver=pdfcov
Published by the AIP Publishing

Förster resonance energy transfer, absorption and emission spectra in multichromophoric systems. I. Full cumulant expansions and system-bath entanglement

Jian Ma and Jianshu Cao[a)]
Department of Chemistry, Massachusetts Institute of Technology, Cambridge, Massachusetts 02139, USA

(Received 13 August 2014; accepted 6 February 2015; published online 3 March 2015)

We study the Förster resonant energy transfer rate, absorption and emission spectra in multichromophoric systems. The multichromophoric Förster theory (MCFT) is determined from an overlap integral of generalized matrices related to the donor's emission and acceptor's absorption spectra, which are obtained via a full 2nd-order cumulant expansion technique developed in this work. We calculate the spectra and MCFT rate for both localized and delocalized systems, and calibrate the analytical 2nd-order cumulant expansion with the exact stochastic path integral method. We present three essential findings: (i) The role of the initial entanglement between the donor and its bath is found to be crucial in both the emission spectrum and the MCFT rate. (ii) The absorption spectra obtained by the cumulant expansion method are nearly identical to the exact spectra for both localized and delocalized systems, even when the system-bath coupling is far from the perturbative regime. (iii) For the emission spectra, the cumulant expansion can give reliable results for localized systems, but fail to provide reliable spectra of the high-lying excited states of a delocalized system, when the system-bath coupling is large and the thermal energy is small. This paper also provides a simple golden-rule derivation of the MCFT, reviews existing methods, and motivates further developments in the subsequent papers. © *2015 AIP Publishing LLC.* [http://dx.doi.org/10.1063/1.4908599]

I. INTRODUCTION

Background. Excitonic energy transfer (EET)[1–5] attracts extensive interest in many subjects. It is a fundamental problem in various physical and chemical processes.[6–10,12] In general, the efficiency of the EET can be well quantified by the Förster resonance energy transfer (FRET) theory[1,2,4] under the following two conditions: (a) The system can be treated as two parts: the donor and acceptor, and the coupling between them is much weaker than the system-bath coupling, i.e., the transfer is usually incoherent. (b) Both acceptor and donor can be treated as point dipoles.

However, the FRET theory is problematic in complex molecular systems such as the light-harvesting complexes LH1/LH2.[9–11] In such systems, the donor and/or acceptor could have more than one chromophore and cannot be treated as point dipoles. Moreover, due to the electronic couplings V^D (V^A) within the donor(acceptor), the excitations are not localized, and their coherent dynamics could be quite important in the EET process,[13–16] which was shown recently in two-dimensional electronic spectroscopy experiments.[17–19] In systems as the LH2 complex, the energy transfer rate is significantly underestimated by the FRET theory.[11,20–22,46] Therefore, the multichromophoric Förster theory (MCFT) was developed by Sumi and others[5,24,25] to describe the coherence within the complexes.

It should be noted that under some experimental conditions, even the extension from the FRET to MCFT may not be sufficient since these theories are 2nd-order with respect to the donor-acceptor coupling J. Nontrivial quantum effects such as multi-site quantum coherence and solvent-controlled transfer can be seen in higher order corrections. We have recently developed a systematic diagrammatic expansion[26] to include high-order corrections that are able to account for the difference between FRET and the full quantum dynamics by including the $O(J^3)$ and $O(J^4)$ terms.

Similar to its single chromophoric counterpart, the MCFT is determined by an overlap integral over the trace of generalized matrices related to the donor's emission and acceptor's absorption spectra. The spectra are broadened and shifted due to the coupling to the environment, which is believed to play a critical role in the EET process of light-harvesting complexes.[27] Unlike the case in the FRET theory, where the spectra can be obtained exactly for an environment with Gaussian fluctuations,[28] the spectra in MC systems are more involved, especially the emission spectrum. This issue is investigated in the article and is systematically resolved both analytically and numerically in subsequent papers.

A. Outline of this paper

Absorption and emission spectra. In the calculation of the MCFT rate, the absorption spectrum is relatively easier to obtain since the initial state is factorized. The emission spectrum is much more complicated due to the initial system-bath coupling, which displaces the bath away from its equilibrium. This displacement will affect the subsequent dynamics, which motivates the subsequent papers and leads to difficulties in evaluating the MCFT rate.

a)jianshu@mit.edu

Donor-bath entanglement. The influence of the initial entanglement, or correlation, between the donor and bath has been widely noticed but lacks systematic study, partially due to the difficulties in numerical techniques. This problem does not exist in the monomer case, where the system is composed of a single electronic state. In this work, we find that the donor-bath entanglement plays a crucial role in both the emission spectrum and MCFT rate. Exact numerical comparisons with stochastic path integral (SPI) techniques show the failure of the two different factorization approaches for both localized and delocalized systems.

Full 2nd-order cumulant expansion (FCE). The primary goal of this series of papers is to develop analytical and numerical techniques to compute the MCFT rate and spectra. Simulation methods such as stochastic path integrals[29] and hierarchy equation of motions (HEOM)[30–33] can give benchmarks for relatively small systems due to the limitation of computing powers. Perturbative methods[5,34–44] are efficient for larger systems but are reliable only in some specific parameter regimes. For example, in the weak system-bath coupling regime, the EET was generally studied by using Green's function,[5] 2nd-order time-convolution (TC2),[25] and time-convolutionless (TCL2) master equations.[34,35]

In this paper, we demonstrate the difficulties and problems in computing the MCFT rates and spectra, and focus on a perturbation approach based on the 2nd-order cumulant expansion. Here, the cumulant expansion is performed on the full system-bath coupling Hamiltonian H_{sb} in both the real- and imaginary-time domains. Then, the absorption and emission spectra are expressed in a FCE, which can reduce to the exact results in the monomer case. As previously shown in the calculation of vibrational spectra,[44,45] factorization of the FCE leads to further approximations that are easy to evaluate analytically. In the exciton basis, H_{sb} will have off-diagonal terms. If the off-diagonal part H_{sb}^{od} is neglected, the FCE reduces to the inverse participation ratio (IPR)[23,41] approximation, which is essentially a pure dephasing model. The IPR method can be improved by treating the off-diagonal elements perturbatively,[44,45] and here, we call this method the off-diagonal cumulant expansion (OCE). In essence, OCE is the cumulant form of the modified Redfield equation without the secular and Markovian approximations.[34,38,39,44,45] The advantage of the FCE over the OCE and IPR methods can be seen in a highly delocalized case, where the omission or perturbation treatment of the off-diagonal coupling is unreliable. For the absorption spectrum, the FCE is formally equivalent to the TCL2, but the TC2 method cannot correctly reduce to the monomer case. For the emission spectrum, neither the TCL2 nor the TC2 method can reduce to the monomer case. The TCL2 method needs the help of a detailed balance identity to overcome this difficult.[35] However, the FCE is straightforward and can reduce to the monomer case naturally.

Reliability. We use the FCE method to calculate the spectra and the MCFT rate for both localized and delocalized systems. For both systems, the FCE method is quite reliable in the absorption spectrum, since there is no population dynamics while the coherence decays rapidly with increasing system-bath coupling.

For the emission spectrum, the FCE method is also reliable when the excitons of the donor are localized, since the FCE is exact for monomers. However, if the donor's excitons are delocalized, the perturbation in imaginary-time is unreliable when the system's energy gap is larger than the thermal energy. In this case, the emission spectrum is only reliable if it is determined by the lower excited states. The MCFT rates are still close to the exact ones since the rate is determined by the spectral overlap.

This paper is organized as follows. In Sec. II, we give the physical model of a multichromophoric system and introduce the MCFT. The role of the initial entanglement is shown by using the exact SPI method. In Sec. III, we derive the absorption and emission spectra by using 2nd-order cumulant expansion techniques. The spectra formula can be further simplified when the system has translational symmetry, and can be reduced to various analytical solutions under further approximations. Then, we calculate the spectra and MCFT rate for localized and delocalized systems, and discuss the reliability of the cumulant expansion method.

B. Outline of the forth-coming papers

The limitation of the FCE method, as well as many other traditional perturbation methods, lies in the poor approximation of the emission spectrum in a delocalized system in the low-temperature and large system-bath coupling regimes. To overcome this problem, several new methods are developed in our group and will appear in the subsequent papers of this series.

(a) For real systems such as the LH2, the energy gaps of the first excitations are comparable to both the thermal energy and the system-bath coupling. None of the traditional perturbation methods can give reliable emission spectra and MCFT rates. For such systems, the treatment of the complex-time system-bath correlation will determine the reliability of the emission spectrum and the MCFT rate. In Paper II,[47] we develop a hybrid cumulant expansion method, which uses the imaginary-time path integrals to obtain the numerically exact reduced density matrix of the donor, from which the displacements of the bath operators can be extracted precisely. Using this method, we can give reliable emission spectrum and MCFT rate of the LH2 system.[29]

(b) Furthermore, to overcome the problems of the HEOM in calculating large systems and low temperature conditions, in our Paper III,[29] we develop a complex-time stochastic PI method, which will provide benchmarks for our calculation. Stochastic PI is not limited to the Drude spectrum and can be used in relatively large systems because it is a wave-function-based method.

(c) Finally, we apply the hybrid cumulant expansion method and the exact stochastic PI to the B850 ring of LH2. The FRET rate, emission and absorption spectra in this realistic system are calculated by considering static disorder, low-temperature effects, and strong system-bath coupling. These exact results for B850 are obtained for the first time and will be reported in Paper IV.[48]

(d) If the system-bath coupling is dominant, even when the donor's excitons are delocalized, perturbation should be made on the donor's off-diagonal coupling V but not the system-bath coupling. This $O(V^2)$ expansion is developed in a future publication.[46]

II. MULTICHROMOPHORIC FRET THEORY

A. Model Hamiltonian

The MCFT describes the resonant energy transfer between a donor (D) and an acceptor (A) in a multichromophoric system, described by the Hamiltonian

$$H = H_t^D + H_t^A + H_c, \tag{1}$$

where H_c is the dipole-dipole coupling between the donor and acceptor, and $H_t^{D(A)}$ is the total Hamiltonian of the donor (acceptor) and its bath,

$$\begin{aligned} H_t^D &= H_s^D + H_{sb}^D + \mathbb{I}_s^D H_b, \\ H_t^A &= H_s^A + H_{sb}^A + \mathbb{I}_s^A H_b. \end{aligned} \tag{2}$$

A schematic picture of the model system is shown in Fig. 1. We first explain the donor's part. The free Hamiltonian of the donor is

$$H_s^D = \sum_{m=1}^{N_D} \left(\epsilon_m^D + \lambda_m^D\right) |D_m\rangle\langle D_m| + \sum_{m\neq n}^{N_D} V_{mn}^D |D_m\rangle\langle D_n|, \tag{3}$$

where ϵ_m^D is the excitation energy of the donor's mth site, and λ_m^D is the reorganization energy induced by the interaction between the bath and the donor's mth chromophore. V_{mn}^D is the coupling between sites m and n. In the MCFT, we focus on the single excitation case and thus, $|D_m\rangle$ represents the state that the total multichromophoric system is excited only at the donor's mth site, while all the other sites (including the acceptor's) are in their ground state, i.e.,

$$|D_m\rangle = |0, \ \ldots 1_m, \ \ldots, \ 0\rangle_D |0\cdots 0\rangle_A. \tag{4}$$

The identity operator $\mathbb{I}_s^D$ is given by

$$\mathbb{I}_s^D = \sum_{m=1}^{N_D} |D_m\rangle\langle D_m|. \tag{5}$$

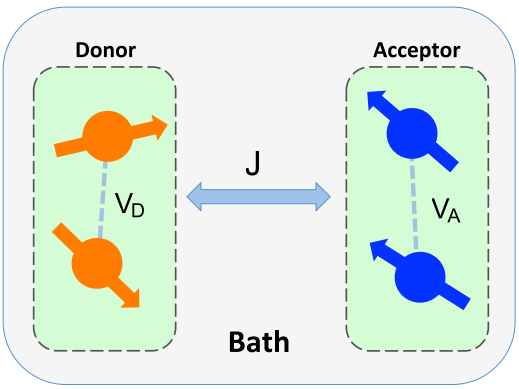

FIG. 1. Schematic picture of a multi-chromophoric system embedded in a bath. The molecules in the donor and acceptor are treated as dipoles, and the coupling between them is J.

In this work, the baths that couple to different chromophores are independent. It is very straightforward to extend the results by using correlated baths, as shown in Refs. 32 and 49. The bath is usually modeled by a set of harmonic oscillators,

$$H_b^D = \sum_{m=1}^{N_D} \sum_k \hbar\omega_{m,k}^D b_{m,k}^{D\dagger} b_{m,k}^D, \tag{6}$$

where $\omega_{m,k}^D$ is the frequency of the kth mode of the bath that is coupled to the mth site of the donor. The excitation states couple with the harmonic bath linearly as

$$H_{sb}^D = \sum_{m=1}^{N_D} \hat{B}_m^D |D_m\rangle\langle D_m|, \tag{7}$$

where the bath operators are given by

$$\hat{B}_m^D = \sum_k g_{m,k}^D \left(b_{m,k}^{D\dagger} + b_{m,k}^D\right). \tag{8}$$

The relation between the coupling strengths $g_{m,k}^D$ and the reorganization energy is $\lambda_m^D \equiv \sum_k g_{m,k}^2/\omega_{m,k}$.

The acceptor's Hamiltonians H_s^A, H_b^A, and H_{sb}^A are obtained by replacing the notation D with A in the above discussion.

The dipole-dipole interaction between the donor and acceptor is given by

$$H_c = \sum_{m=1}^{N_D} \sum_{n=1}^{N_A} J_{mn} |D_m\rangle\langle A_n|, \tag{9}$$

where the couplings J_{mn} are treated perturbatively in the MCFT.

B. Golden-rule formulation of the MCFT rate

To formulate the MCFT rate k, we should understand the time scales in the energy transfer process. The MCFT describes the incoherent transfer of excitations from a donor to an acceptor. This transfer happens after the donor is excited to its single excitation manifold. In general, the donor's initial excitations will relax to an equilibrium state with its bath on a time scale that is much shorter than the excitation transfer time $1/k$. Therefore, the initial condition of the MCFT process can be considered as an equilibrium state of the donor and its bath. On the other hand, the lifetime of the first excitations are usually much longer than the excitation transfer time, and thus the ground state is not involved in the MCFT.

Based on the above conditions, the MCFT rate can be derived straightforwardly from Fermi's golden rule,[5]

$$k = 2\pi \sum_{\mu\nu} P_\nu^D \left|\langle\Psi_\nu^D|H_c|\Phi_\mu^A\rangle\right|^2 \delta\left(E_\nu^D - E_\mu^A\right), \tag{10}$$

where $|\Psi_\nu^D\rangle$ ($|\Phi_\mu^A\rangle$) and E_ν^D (E_μ^A) are the eigenstates and eigenenergies of H_t^D (H_t^A), which include the degrees of freedom of both the system and bath. P_ν^D is obtained from

$$\rho^D = \rho_e^D \rho_b^A = \sum_\nu P_\nu^D |\Psi_\nu^D\rangle\langle\Psi_\nu^D|, \tag{11}$$

where

$$\rho_e^D = \frac{e^{-\beta H^D}}{\mathrm{tr} e^{-\beta H^D}},\ \rho_b^A = \frac{e^{-\beta H_b^A}}{\mathrm{tr} e^{-\beta H_b^A}}, \tag{12}$$

and $\beta^{-1} = k_B T$, with k_B the Boltzmann's constant and T the temperature.

Starting from Eq. (10), the MCFT rate can be derived as

$$k = \sum_{m,n}\sum_{m'n'} J_{mn}J_{m'n'}\int_{-\infty}^{\infty} dt\, \mathrm{tr}_b\{e^{iH_t^D t}\rho_e^D\rho_b^A \times |D_{m'}\rangle\langle A_{n'}|e^{-iH_t^{A_t}t}|A_n\rangle\langle D_m|\}, \tag{13}$$

and since the degrees of freedom of the acceptor and donor can be treated separately,

$$k = \sum_{m,n}\sum_{m'n'} J_{mn}J_{m'n'}\int_{-\infty}^{\infty} dt \times \mathrm{tr}_{bA}\left[\rho_b^A e^{iH_b^{A_t}t}\langle A_{n'}|e^{-iH^{A_t}t}|A_n\rangle\right] \times \mathrm{tr}_{bD}\left[\langle D_m|e^{iH^{D_t}t}\rho_e^D|D_{m'}\rangle e^{-iH_b^{D_t}t}\right]. \tag{14}$$

Now, we can define two matrices

$$\mathbf{I}^A(t) = \mathrm{tr}_b\left(e^{-iH^{A_t}t}\rho_b^A e^{iH_b^{A_t}t}\right), \tag{15}$$

$$\mathbf{E}^D(t) = \mathrm{tr}_b\left(e^{iH^{D_t}t}\rho_e^D e^{-iH_b^{D_t}t}\right), \tag{16}$$

and the MCFT rate can be expressed as

$$k = \int_{-\infty}^{\infty} dt\, \mathrm{tr}\left[\mathbf{J}^T\mathbf{E}^D(t)\,\mathbf{J}\mathbf{I}^A(t)\right], \tag{17}$$

where

$$\mathbf{J} = \sum J_{mn}|D_m\rangle\langle A_n|. \tag{18}$$

It is important to notice that the density matrix appearing in $\mathbf{I}^A(t)$ is the thermal equilibrium state of the acceptor's bath. The donor is assumed to be in its excited equilibrium state ρ_e^D. This non-factorized initial state brings technical difficulties in the calculation of the emission spectrum, especially when the system-bath coupling is strong. The primary goal of this series of papers is to develop analytical and numerical techniques to compute the donor-bath correlations.

The absorption and emission matrices are given by

$$\begin{aligned}\mathbf{I}^A(\omega) &= \int_{-\infty}^{\infty} dt\, e^{i\omega t}\mathbf{I}^A(t),\\ \mathbf{E}^D(\omega) &= \int_{-\infty}^{\infty} dt\, e^{-i\omega t}\mathbf{E}^D(t),\end{aligned} \tag{19}$$

which satisfy the normalization conditions $\mathrm{tr}\mathbf{I}^A(t=0) = N$ and $\mathrm{tr}\mathbf{E}^D(t=0) = 1$. Thus, the MCFT rate can also be written as[5,25]

$$k = \frac{1}{2\pi}\int_{-\infty}^{\infty} d\omega\, \mathrm{tr}\left[\mathbf{J}^T\mathbf{E}^D(\omega)\,\mathbf{J}\mathbf{I}^A(\omega)\right]. \tag{20}$$

From the above formula, the rate k is determined by the donor-acceptor coupling $\mathbf{J}$, and the overlap integral of the acceptor's absorption matrix $\mathbf{I}^A_{nn'}(\omega)$, and the donor's emission matrix $\mathbf{E}^D_{m'm}(\omega)$. The influences of the system-bath coupling on the transfer rate are reflected by the spectra in their widths and positions, which are determined by the relaxation dynamics and reorganization energies, respectively. Therefore, the main problem here is to calculate the spectra. The spectra (19) in the MCFT rate do not depend on the system's local dipoles. Actually, the commonly studied far-field spectra $I_{\mathrm{f}}^A(\omega)$ and $E_{\mathrm{f}}^D(\omega)$ can be obtained as

$$\begin{aligned}I_{\mathrm{f}}^A(\omega) &= \sum_{m,n}(\hat{\epsilon}\cdot\vec{\mu}_m^A)(\hat{\epsilon}\cdot\vec{\mu}_n^A)\, I_{mn}^A(\omega),\\ E_{\mathrm{f}}^D(\omega) &= \sum_{m,n}(\hat{\epsilon}\cdot\vec{\mu}_m^D)(\hat{\epsilon}\cdot\vec{\mu}_n^D)\, E_{mn}^D(\omega),\end{aligned} \tag{21}$$

where $\hat{\epsilon}$ is the polarization of the light and $\vec{\mu}_i$ denote the local dipole operators.

In this work, for the sake of simplicity, the donor-acceptor coupling is assumed to be constant, $J_{mn} = J$. Therefore, the MCFT rate formula (20) can be simplified as

$$k = \frac{J^2}{2\pi\hbar^2}\int_{-\infty}^{\infty} d\omega E^D(\omega)\, I^A(\omega), \tag{22}$$

where

$$\begin{aligned}E^D(\omega) &= \sum_{m,n} E_{mn}^D(\omega),\\ I^A(\omega) &= \sum_{m,n} I_{mn}^A(\omega).\end{aligned} \tag{23}$$

We should emphasize that the exact rate formula should refer to Eq. (20).

III. EFFECTS OF DONOR-BATH ENTANGLEMENT

In the MCFT, the donor is first excited to its single-excitation subspace, which relaxes to equilibrium with its bath in a time scale that is negligibly small as compared with the EET time. Therefore, the initial state is an equilibrium state of the donor and its bath, as shown in Eq. (16). In this case, the donor and its bath are usually correlated or entangled due to their interaction, which is characterized by the reorganization energy λ.

When λ is smaller than the system's energy scale, or the bath correlation time is negligibly small (e.g., in the high-temperature limit), the Born approximation is employed and a master equation is obtained. However, when the system-bath interaction is larger than the other energy scales, the Born approximation is invalid, and the composite system-bath state cannot be factorized during the entire MCFT process. To our knowledge, only a few methods can treat the system-bath correlation exactly. Here, we first use the HEOM method to show the crucial role of the donor-bath entanglement. The 2nd-order correction of the initial state is studied in Sec. IV C.

In this work, both the donor and acceptor consist of two chromophores, respectively. Since the entanglement is determined by the properties of the system, we consider two limiting cases. In Case I, the system is localized, and its Hamiltonian is (in the unit of cm^{-1})

$$H_s^{D1} = \begin{pmatrix}250 & 20\\ 20 & 150\end{pmatrix},\ H_s^{A1} = \begin{pmatrix}100 & 20\\ 20 & 0\end{pmatrix}, \tag{24}$$

where the ratio of the excitation energy difference $\Delta = E_2 - E_1$ to the inter-chromophore coupling V is $\Delta/V = 5$. In Case II, the

system is delocalized ($\Delta/V = 0.2$),

$$H_s^{D2} = \begin{pmatrix} 200 & 100 \\ 100 & 180 \end{pmatrix}, \; H_s^{A2} = \begin{pmatrix} 100 & 100 \\ 100 & 80 \end{pmatrix}. \tag{25}$$

The influence of the bath on the system dynamics is determined by the system-bath coupling spectrum; here, we choose the Drude spectrum

$$J(\omega) = \frac{2\lambda\omega\gamma}{\omega^2 + \gamma^2}, \tag{26}$$

where λ is the reorganization energy and γ is the cutoff frequency of the bath. For the sake of simplicity, the reorganization energies are the same for each site. The donor-acceptor coupling is $J_{mn} = J = 10\ \mathrm{cm}^{-1}$.

To study the effects of the initial entanglement, we consider three different treatments of the initial state:

(i) The initial state is obtained exactly by using the HOEM. In this case, the system and bath first evolved to equilibrium. Then, the system and bath evolve according to Eq. (16). The emission spectrum obtained in this case is exact.[33]

(ii) The initial state is factorized, but the system's reduced density matrix is exact,

$$\rho(0) = \rho_{\mathrm{ex}}^D \rho_b^D, \tag{27}$$

where ρ_{ex}^D is the exact reduced density matrix of the donor, and $\rho_b^D = \exp\left(-\beta H_b^D\right)/Z_b^D$ is the equilibrium state of the bath. In this case, we use the HEOM method to obtain the exact reduced density matrix, then all the auxiliary fields are reset to zero. Thus, the correlation between system and bath is turned off. Alternatively, we can obtain the reduced density matrix directly using the imaginary-time path integral method.[50]

(iii) The initial state is also factorized as

$$\rho(0) = \rho_{\mathrm{eq}}^D \rho_b^D; \tag{28}$$

however, $\rho_{\mathrm{eq}}^D = \exp\left(-\beta H_s^D\right)/Z_s^D$ is the thermal equilibrium state of donor. This is also the initial state commonly used in master equation methods.

The comparison of the emission spectra $E^D(\omega)$ for different initial states is shown in Fig. 2. Because the reorganization energy $\lambda = 100\ \mathrm{cm}^{-1}$ is comparable to the excitation energies, the separable approximation is not reliable. For the localized system (Case I), the spectra obtained by the separable approximations are shifted with respect to the exact result due to the neglect of reorganization effects. The delocalized system (Case II) is more interesting, where the double-peak structure seen in the exact result disappears in the approximate spectra. The entanglement effect in the delocalized case is more noticeable than in the localized one. Only in the limiting case where the system is fully localized, i.e., the intermolecular coupling $V = 0$ and thus the chromophores are independent, there is no entanglement between the donor and its bath. In this case, the initial state can be written as

$$\rho(0) = \rho_{\mathrm{eq}}^D \tilde{\rho}_b^D, \tag{29}$$

where $\tilde{\rho}_b^D$ is the equilibrium state of the displaced bath.

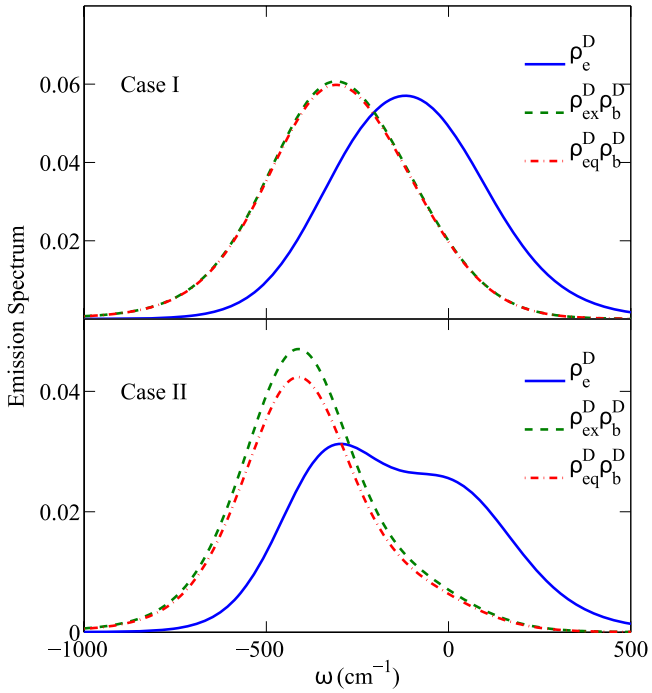

FIG. 2. Comparison of the emission spectra for different initial states in localized (Case I) and delocalized (Case II) systems. The reorganization energy $\lambda = 100\ \mathrm{cm}^{-1}$, the cutoff frequency $\gamma = 10\ \mathrm{ps}^{-1}$, and the temperature $T = 300$ K.

The effects of initial entanglement on the MCFT rate is shown in Fig. 3. For both the localized and delocalized cases, the factorized initial state approximation breaks down rapidly with the increase of the system-bath coupling. It is interesting to note that, in the delocalized case (lower panel), the MCFT rates obtained from $\rho_{\mathrm{ex}}^D\rho_b^D$ and $\rho_{\mathrm{eq}}^D\rho_b^D$ differ dramatically for very large λ, which reflects the deviation of ρ_{ex}^D and ρ_{eq}^D. As the entanglement plays such a notable role, we should treat the initial state in a more accurate way, such as through the cumulant expansion method used below and the hybrid cumulant expansion method developed in Paper II.

IV. SECOND-ORDER CUMULANT EXPANSION

In this section, we derive the FCE formulas of the absorption and emission spectra. The absorption and emission spectra were studied by various methods, such as the standard TC2[25] and TCL2.[35] The TC2 method is time-nonlocal and does not recover the simple case of monomers. As shown here and in several previous calculations, the TC2 approximation[25] fails to reproduce the detailed structures of line-shapes and can lead unphysical peaks in the spectrum. The TCL2 method is time-local and recovers the exact solution for the absorption spectrum of monomers. In this framework, the TCL2 approximation of the emission spectrum has an inhomogeneous term that describes the unfactorized initial state, but it cannot give the exact results in the monomer limit for emission. A detailed balance identity should be used to overcome this difficulty.[35] For the absorption spectrum, the FCE method shown below is the same as the TCL2 method. For the emission spectrum, the cumulant expansion method can reduce to the monomer case,

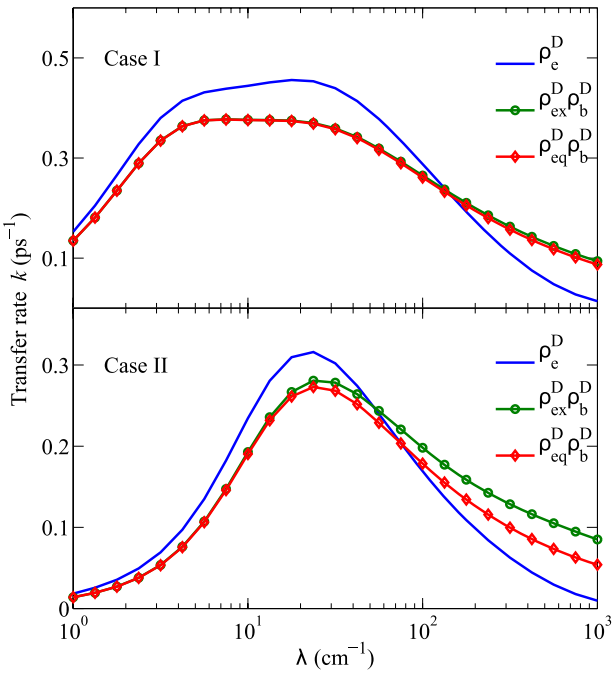

FIG. 3. Comparison of the MCFT rate as a function of the reorganization energy λ from 1 cm^{-1} to 1000 cm^{1} for different initial states. All the other parameters are the same as in Fig. 2.

and can easily give the equivalent results as shown in Ref. 35, but without the help of the additional detailed balance identity.

A. Absorption spectrum: Full 2nd-order cumulant expansion

Below, we derive the absorption spectrum via 2nd-order cumulant expansion. It is convenient to diagonalize the acceptor's Hamiltonian H_s^A at first,

$$H_s^A = \sum_{\mu=1}^{N_A} \epsilon_\mu^A |\mu\rangle\langle\mu|, \tag{30}$$

where ϵ_μ^A is the eigenenergy (containing λ),

$$|\mu\rangle = \sum_{i=1}^{N_A} c_i^\mu |A_i^e\rangle \tag{31}$$

is the energy eigenstate (the exciton), and $c_i^\mu = \langle\mu|A_i^e\rangle$. However, in the energy representation the system-bath coupling has off-diagonal terms,

$$H_{sb}^A = \sum_{\mu,\nu=1}^{N_A} \tilde{B}_{\mu\nu}^A |\mu\rangle\langle\nu|, \tag{32}$$

where

$$\tilde{B}_{\mu\nu}^A = \sum_{n=1}^{N_A} X_n^{\mu\nu} \hat{B}_n^A \tag{33}$$

and the coefficient $X_n^{\mu\nu} = c_n^\mu c_n^{\nu *}$. Below, we perform a cumulant expansion with respect to H_{sb}^A. In Refs. 44 and 45, the cumulant expansion was carried out with respect to the off-diagonal terms of the Hamiltonian H_{sb}^A (32), which could yield unreliable results in highly delocalized cases.

The 2nd-order cumulant expansion of H_{sb}^A of Eq. (15) gives

$$\mathbf{I}^A(t) \simeq e^{-iH_s^A t} e^{-\mathbf{K}(t)}, \tag{34}$$

where the time-dependent matrix

$$\begin{aligned}\mathbf{K}(t) &= \int_0^t dt_2 \int_0^{t_2} dt_1 \mathrm{tr}_b \left[H_{sb}^A(t_2) H_{sb}^A(t_1) \rho_b^A\right] \\ &= \sum_{\mu,\nu=1}^{N_A} |\mu\rangle\langle\nu| \sum_{\alpha=1}^{N_A}\sum_{n=1}^{N_A} X_n^{\mu\alpha} X_n^{\alpha\nu} \\ &\quad \times \int_0^t dt_2 \int_0^{t_2} dt_1 e^{i\omega_{\mu\alpha}t_2 - i\omega_{\nu\alpha}t_1} C_n^B(t_2 - t_1), \end{aligned} \tag{35}$$

where $\omega_{ij} \equiv \epsilon_i - \epsilon_j$ and

$$H_{sb}^A(t) \equiv e^{i(H_s^A + H_b^A)t} H_{sb}^A e^{-i(H_s^A + H_b^A)t}. \tag{36}$$

The time-correlation function of the bath $C_n^B(t_2 - t_1) \equiv \mathrm{tr}_b \left[B_n^A(t_2) B_n^A(t_1) \rho_b^A\right]$ is time translational invariant. In a general case if we have a complex time $\theta = s - i\tau$, the correlation function can be expressed as

$$C_n^B(\theta) = \int_0^\infty \frac{d\omega}{\pi} J_n(\omega) \frac{\cosh\left[\omega\left(\frac{1}{2}\beta - i\theta\right)\right]}{\sinh\left[\frac{1}{2}\omega\beta\right]}, \tag{37}$$

where $J_n(\omega)$ is the spectral density of bath coupled to the nth site. In this paper, we choose Drude spectrum (26) and assume the reorganization energies are the same for different baths, i.e., $J(\omega) = J_n(\omega)$.

The calculation of the absorption spectra $I_A(\omega)$ for localized (24) and delocalized (25) systems is shown in Figs. 4 and 6, respectively. We know that if the system is fully localized, i.e., $V_{ij}^{D(A)} = 0$, the cumulant expansion method is exact. Since the Hamiltonian (24) does not deviate from the fully localized case very much, the cumulant expansion method can give very precise results, as shown in Fig. 4. The cumulant expansion results for the delocalized system are also in good agreement with the exact spectra obtained by the stochastic PI method, even for a very large reorganization energy $\lambda = 500$ cm^{-1}.

B. Absorption spectrum: Further reduction of the FCE method to other analytical solutions

To evaluate Eq. (34), we need to diagonalize the matrix $\mathbf{K}(t)$. In practice, we can avoid the diagonalization by making further approximations, such as the IPR. In a previous study of vibrational spectra,[45] we arrived at similar expressions and by factoring the contribution from the diagonal and off-diagonal parts of the interaction Hamiltonian

$$H_{sb}^A = H_{sb}^{A,d} + H_{sb}^{A,od}, \tag{38}$$

in the exciton bases, where $H_{sb}^{A,d}$ and $H_{sb}^{A,od}$ are the diagonal and off-diagonal parts.

1. IPR approximation: Pure dephasing model

If we neglect $H_{sb}^{A,od}$ and perform cumulant expansion on the diagonal part $H_{sb}^{A,d}$ only, we will arrive at the IPR

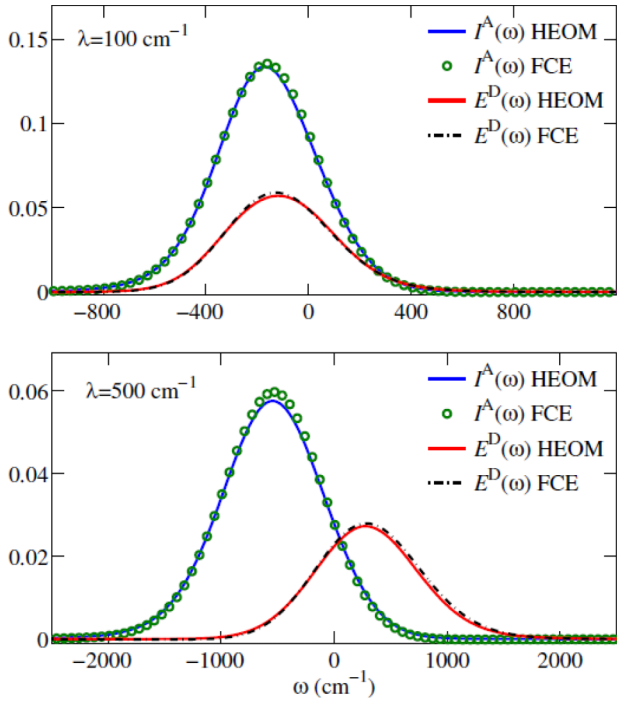

FIG. 4. Absorption and emission spectra of the localized system [Case I defined in (24)]. Results are obtained by using the FCE and stochastic PI methods. The bath parameters are the same as in Fig. 2. Even for a very large reorganization energy $\lambda = 500$ cm^{-1}, the FCE results are in very good agreement with the exact one.

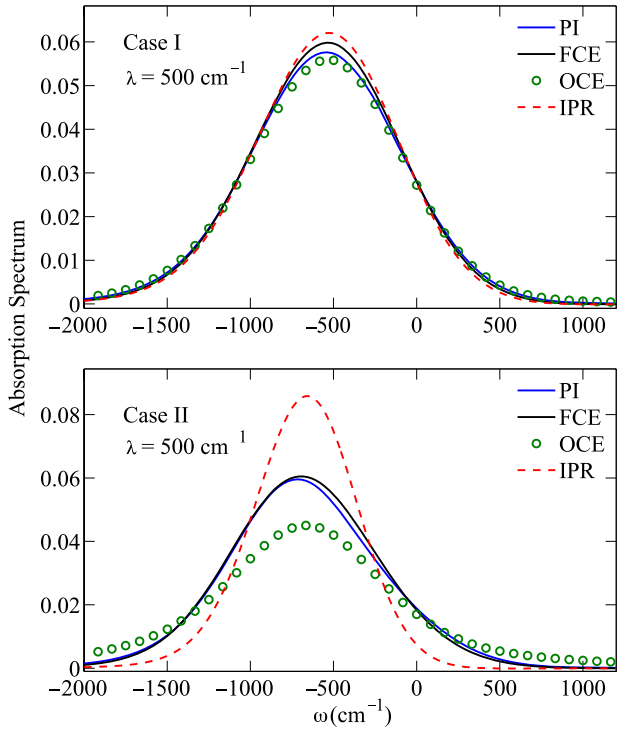

FIG. 5. Absorption spectra obtained via the stochastic PI, FCE, OCE, and IPR methods. The OCE and IPR methods fail to give reliable results in the delocalized case.

method,[11,23] and the absorption spectrum is calculated as

$$\mathbf{I}^A_{IPR}(t) \simeq \sum_\mu |\mu\rangle\langle\mu| \exp\left[-i\epsilon^A_\mu t - K^{IPR}_{\mu\mu}(t)\right], \quad (39)$$

where

$$K^{IPR}_{\mu\mu}(t) = \sum_{n=1}^{N_A} \left|X^{\mu\mu}_n\right|^2 \int_0^t dt_2 \int_0^{t_2} dt_1 C^B(t_2 - t_1). \quad (40)$$

We should note that $K^{IPR}_{\mu\mu}(t)$ is not the diagonal part of $\mathbf{K}(t)$ in Eq. (35), as the latter incorporates the contributions from both diagonal and off-diagonal parts of the interaction Hamiltonian. Essentially, the IPR approximation is a pure dephasing model, which accounts only for the diagonal fluctuations. It is reliable only for the localized case, in which the off-diagonal terms of the system-bath coupling are small.

2. OCE approximation: Modified Redfield approach

Further improvement can be made by including the contribution from $H^{A,od}_{sb}$. Actually, the diagonal part of $\mathbf{K}(t)$ can be written as

$$K_{\mu\mu}(t) = K^{IPR}_{\mu\mu}(t) + \sum_{\alpha\neq\mu} R_{\mu\alpha\alpha\mu}(t), \quad (41)$$

where the Redfield tensor

$$R_{\mu\alpha\alpha\mu}(t) = \sum_{\alpha\neq\mu}\sum_{n=1}^{N_A} \left(X^{\mu\alpha}_n\right)^2 \times \int_0^t dt_2 \int_0^{t_2} dt_1 e^{i\omega_{\mu\alpha}(t_2-t_1)} C(t_2 - t_1) \quad (42)$$

describes the transition from state α to μ, which is induced by the off-diagonal part of the acceptor-bath interaction Hamiltonian $H^{A,od}_{sb}$. Therefore, the absorption spectrum can also be given as

$$\mathbf{I}^A_{OCE}(t) \simeq \sum_\mu |\mu\rangle\langle\mu| \exp\left[-i\epsilon^A_\mu t - K^{IPR}_{\mu\mu}(t) - \sum_{\alpha\neq\mu} R_{\mu\alpha\alpha\mu}(t)\right], \quad (43)$$

which is the OCE approach. In essence, the OCE approach is equivalent to the cumulant version of the modified Redfield equation, as both approaches treat the diagonal part of the system-bath coupling exactly and the off-diagonal part perturbatively.[34,38,39,44,45]

The FCE, OCE, and IPR are compared in Fig. 5. For localized systems, all of the approximations give reliable results. However, for the delocalized case, since the off-diagonal terms of $H^{D(A)}_{sb}$ are not negligible, only the FCE can give accurate absorption spectra.

3. Markovian and secular approximations

In condensed phase spectroscopy, the diagonal part of the system-bath coupling leads to pure dephasing and the off-diagonal part leads to population relaxation. If we adopt the Markovian and secular approximations, the FCE or OCE expression reduces to the standard result,

$$\mathbf{I}^A(t) \simeq \sum_\mu |\mu\rangle\langle\mu| \exp\left[-i\epsilon^A_\mu t - \Gamma^{dep}_{\mu\mu} t - \sum_{\alpha\neq\mu} \Gamma^{rel}_{\mu\alpha} t\right], \quad (44)$$

where Γ^{dep} and Γ^{rel} are the dephasing and population relaxation rates, respectively. We obtain these Markovian rates by taking the long time limit of the Redfield tensers: $R_{\mu\mu\mu\mu}(t) \equiv \Gamma^{dep}_{\mu\mu} t$ and $R_{\mu\alpha\alpha\mu}(t) \equiv \Gamma^{rel}_{\mu\alpha} t$. Since pure dephasing is usually fast and dominant, we can retain the full treatment of pure dephasing and apply the Markov-secular treatment to population relaxation. Then, the absorption spectrum is also given as

$$\mathbf{I}^A(t) \simeq \sum_{\mu} |\mu\rangle\langle\mu| \exp\left[-i\epsilon^A_{\mu} t - K^{IPR}_{\mu\mu}(t) - \sum_{\alpha\neq\mu} \Gamma^{rel}_{\mu\alpha} t\right], \quad (45)$$

which can achieve accuracy comparable to OCE and efficiency comparable to IPR.

C. Emission spectrum

Here, we will derive the emission spectrum in the exciton basis. As discussed in Sec. III, the system-bath entanglement is crucial in the calculation of the emission spectrum, and here, we treat the expand the density matrix ρ^D_e in Eq. (16) to 2nd-order in the system-bath coupling. We first consider the partition function $Z^D_e = \mathrm{tr}\left(e^{-\beta H^D}\right)$, which is given in the cumulant expansion by

$$Z^D_e \simeq Z^D_b \mathrm{tr}_D\left[e^{-\beta H^D_s} e^{\mathbf{K}^{II}(\beta)}\right], \quad (46)$$

where the matrix

$$\begin{aligned}\mathbf{K}^{II}(\beta) &= \int_0^{\beta} d\tau_2 \int_0^{\tau_2} d\tau_1 \mathrm{tr}_b\left[H^D_{sb}(-i\tau_2) H^D_{sb}(-i\tau_1) \rho^D_b\right] \\ &= \sum_{\mu\nu\alpha}\sum_n X^{\mu\alpha}_n X^{\alpha\nu}_n |\mu\rangle\langle\nu| \\ &\quad \times \int_0^{\beta} d\tau' e^{\omega_{\mu\nu}\tau'} \int_0^{\tau'} d\tau\, e^{\omega_{\nu\alpha}\tau} C^B(-i\tau), \quad (47)\end{aligned}$$

and the imaginary time bath correlation function $C^B(-i\tau)$ is given by Eq. (37). After similar algebra used in Sec. IV B, we obtain

$$\mathbf{E}_D(t) \simeq \frac{e^{-(\beta+it)H^D_s} e^{-\mathbf{K}^{RR}(t,\beta)+i\mathbf{K}^{RI}(t,\beta)+\mathbf{K}^{II}(\beta)}}{\mathrm{tr}_D\left[e^{-\beta H^D_s} e^{\mathbf{K}^{II}(\beta)}\right]}, \quad (48)$$

where

$$\begin{aligned}\mathbf{K}^{RR}(t,\beta) &= \int_0^t ds_2 \int_0^{s_2} ds_1 \mathrm{tr}_b\left[H^D_{sb}(s_2 - i\beta)\right. \\ &\quad \left. \times H^D_{sb}(s_1 - i\beta)\rho^D_b\right] \\ &= \sum_{\mu\nu\alpha}\sum_n X^{\mu\alpha}_n X^{\alpha\nu}_n |\mu\rangle\langle\nu| e^{\beta\omega_{\mu\nu}} \\ &\quad \times \int_0^t ds' e^{i\omega_{\mu\nu}s'} \int_0^{s'} ds\, e^{i\omega_{\nu\alpha}s} C^B(s) \quad (49)\end{aligned}$$

and

$$\begin{aligned}\mathbf{K}^{RI}(t,\beta) &= \int_0^t ds \int_0^{\beta} d\tau \mathrm{tr}_b\left[H^D_{sb}(s - i\beta) H^D_{sb}(-i\tau)\rho^D_b\right] \\ &= \sum_{\mu\nu\alpha}\sum_n X^{\mu\alpha}_n X^{\alpha\nu}_n |\mu\rangle\langle\nu| e^{\beta\omega_{\mu\alpha}} \\ &\quad \times \int_0^t ds \int_0^{\beta} d\tau e^{i\omega_{\mu\alpha}s - \omega_{\nu\alpha}\tau} C^B(-s - i\tau). \quad (50)\end{aligned}$$

We note that matrices $\mathbf{K}^{RR}(t,\beta)$ and $\mathbf{K}^{RI}(t,\beta)$ depend both on time and temperature, which reflect that the dynamics is affected by the initial system-bath correlation. The explicit forms of the above matrices for the Drude spectrum are given in the Appendix.

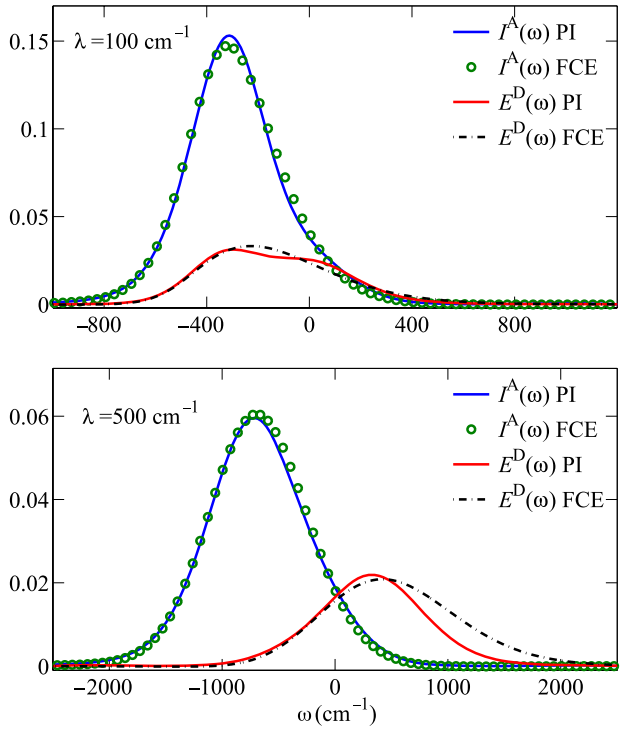

FIG. 6. Absorption and emission spectra of the delocalized system (25). We compare the results of the FCE and the stochastic PI methods. The bath parameters are the same as in Fig. 2.

The comparisons of the emission spectra $E^D(\omega)$ for localized [Case I (24)] and delocalized [Case II (25)] systems are shown in Figs. 4 and 6, respectively. For a localized system, the donor and its bath is weakly entangled, thus the cumulant expansion method performs very well, as shown in Fig. 4. For a delocalized system, the donor and its bath could be strongly entangled. The emission spectra deviate from the exact one when the system-bath coupling becomes so strong that the initial state is far from a factorized state. Actually, perturbative methods are unreliable in this parameter regime. The reliability of the cumulant expansion method will be discussed in Sec. IV E.

D. Systems with translational symmetry

To calculate the emission and absorption spectra, we need to diagonalize all the **K** matrices at every time step according to Eqs. (34) and (48). This could be time consuming if the system is large. Fortunately, it can be proved that the matrices **K** are diagonal when a system has translational symmetry and the reorganization energies are also equal.

All the **K** matrices have the factor

$$\sum_n X^{\mu\alpha}_n X^{\alpha\nu}_n = \sum_n \langle\mu|n\rangle |\langle n|\alpha\rangle|^2 \langle n|\nu\rangle. \quad (51)$$

If the system has translational symmetry, then

$$|\langle n|\alpha\rangle|^2 = |\langle n+k|\alpha\rangle|^2 = \mathrm{const}. \quad (52)$$

and

$$\sum_n X_n^{\mu\alpha} X_n^{\alpha\nu} = |\langle n|\alpha\rangle|^2 \delta_{\mu\nu}. \tag{53}$$

Therefore, all the off-diagonal terms are zero and the matrix becomes diagonal.

Usually, real systems do not have perfect translational symmetries but have some defects or static disorders. In such cases, the system can be described by H_0, which has perfect translational symmetry, plus δV, which breaks this symmetry. If δV can be treated as a perturbation, it is easy to show that the off-diagonal terms of $\mathbf{K}$ are of order $O\left(\delta V^4\right)$ and can be omitted safely.

E. Reliability of the cumulant expansion for the emission spectrum

The emission spectra shown in Fig. 6 indicate that the cumulant expansion can be problematic when the donor is highly delocalized. However, the cumulant expansion of the absorption spectra is still quite reliable in this case. The most significant difference between the emission and absorption spectra lies in the initial states. For the absorption spectrum, the initial state is factorized and the bath is Gaussian. This Gaussian property is captured quite well by the 2nd-order cumulant expansion. For the emission spectrum, the initial state is entangled and the deviation of the donor's bath from a Gaussian bath is determined by the reorganization energy, which can be viewed as a displacement to the bath. Below, we will analyze the condition that the cumulant expansion is unreliable for the emission spectrum.

According to the Hamiltonian (7), the bath operator couples with the donor's site operator independently. Therefore, when the donor is highly localized, each bath operator is approximately displaced by the scalar reorganization energy. After this displacement, the bath is still Gaussian and the cumulant expansion is safe. However, if the donor is highly delocalized, the displacement is no longer a scalar quantity, and the bath is not Gaussian. This problem becomes serious when the donor's energy gap is larger than the thermal energy, i.e., $\left|\beta H_s^D\right| > 1$. In this case, the cumulant expansion of the imaginary-time part is unreliable. We should note that this is the case in LH2, even when $T = 300$ K.

Below, we give a concrete example to illustrate this problem. We consider a fully delocalized donor,

$$H_s^D = \begin{pmatrix} 0 & V \\ V & 0 \end{pmatrix}. \tag{54}$$

For this system, as we just showed in Sec. IV D the matrices $\mathbf{K}^{II}$, $\mathbf{K}^{RR}$ and $\mathbf{K}^{RI}$ are diagonal in the energy representation.

The matrix $\mathbf{K}^{RR}$ is obtained from the 2nd-order cumulant expansion of the real-time part. It depends on both the time and the temperature. According to Eqs. (49) and (53), since the donor's Hamiltonian (54) here has translational symmetry, $\mathbf{K}^{RR}$ is diagonal, and it does not depend on the temperature. This term should be reliable since we obtain very accurate absorption spectra in this case as shown in Figs. 4 and 6. $\mathbf{K}^{II}$ comes from the 2nd-order correction of the equilibrium state and is unreliable for the low-temperature case.

The matrix $\mathbf{K}^{RI}$ comes from the first-order correction of the real-time part and the first-order correction of the imaginary-time (temperature) part. It is diagonal when we use the Hamiltonian (54), and the diagonal elements are

$$K_{\mu\mu}^{RI} \simeq i\frac{2\lambda}{\beta} e^{-\gamma t} \sum_{\alpha=1}^{N_D} \frac{e^{i\omega_{\mu\alpha}(t-i\beta)}}{\lambda^2 + \omega_{\mu\alpha}^2}, \tag{55}$$

where the Drude spectrum (26) and the high-temperature limit $\cot\frac{\beta\gamma}{2} \simeq \frac{2}{\beta\gamma}$ are used (see the Appendix). From the above expression, we see that all the excited states $|\alpha\rangle$ will contribute to the matrix element $K_{\mu\mu}^{RI}$.

The summation of α in Eq. (55) can be divided into two parts: (i) $\mu > \alpha$, and thus $\exp\left(\beta\omega_{\mu\alpha}\right) > 1$. (ii) $\mu \le \alpha$, and thus $\exp\left(\beta\omega_{\mu\alpha}\right) \le 1$. If $|\mu\rangle$ is a low-lying excited state, we have $\exp\left(\beta\omega_{\mu\alpha}\right) \le 1$ for most α, and $K_{\mu\mu}^{RI}$ will not become a very large value. On the opposite side, if $|\mu\rangle$ is a highly-excited state, $\omega_{\mu\alpha}$ could be a very large positive value and $\exp\left(\beta\omega_{\mu\alpha}\right) \gg 1$. In this case, the matrix element $K_{\mu\mu}^{RI}$ could result in an unreliable dynamics of $E_{\mu\mu}^D(t)$.

Consider the Hamiltonian (54), we can obtain

$$\begin{aligned} K_{11}^{RI} &\simeq i\frac{2\lambda e^{-\gamma t}}{\beta}\left(\frac{1}{\lambda^2} + \frac{e^{-2iVt}}{\lambda^2+\omega_{\mu\alpha}^2} e^{-2\beta V}\right), \\ K_{22}^{RI} &\simeq i\frac{2\lambda e^{-\gamma t}}{\beta}\left(\frac{1}{\lambda^2} + \frac{e^{2iVt}}{\lambda^2+\omega_{\mu\alpha}^2} e^{2\beta V}\right), \end{aligned} \tag{56}$$

where K_{22}^{RI} contains a term that diverges as $\exp(2\beta V)$. In the energy representation, since all the matrices $\mathbf{K}^{II}$, $\mathbf{K}^{RR}$, and $\mathbf{K}^{RI}$ are diagonal, the emission spectrum matrix $\mathbf{E}^D(\omega) = \sum_\mu E_{\mu\mu}^D(\omega)|\mu\rangle\langle\mu|$ is also diagonal. In Fig. 7, we show the deviation of the emission spectra $E_{\mu\mu}^D(\omega)$ obtained by the cumulant expansion and the SPI for different off-diagonal coupling V strengths. The upper two panels show the emission spectrum of the lower level $\mu = 1$, for which the spectrum obtained by the cumulant expansion method is very reliable for different off-diagonal coupling strengths. However, from the lower panels of Fig. 7, the spectrum $E_{22}^D(\omega)$ obtained from the cumulant expansion deviates from the exact one with the increase of V.

Therefore, if the emission spectrum is dominated by the excited states that are below the thermal energy, the cumulant expansion method is still reliable. This is the case when we calculate some far-field emission spectra, where the system's dipole operators will select the lowest excited state.

F. MCFT rate

After the study of spectra, we can calculate the MCFT rate. In Fig. 8, we compare the multichromophoric FRET rate obtained via different methods. The exact results are obtained by the stochastic PI. In this paper, the cumulant expansion is performed with respect to λ. We can also do perturbation with respect to the inter-site coupling V of Eq. (3). This approach[46] has a precision of $O\left(V^2\right)$, as shown in Fig. 8. For a localized system, V is a good perturbative parameter, while for

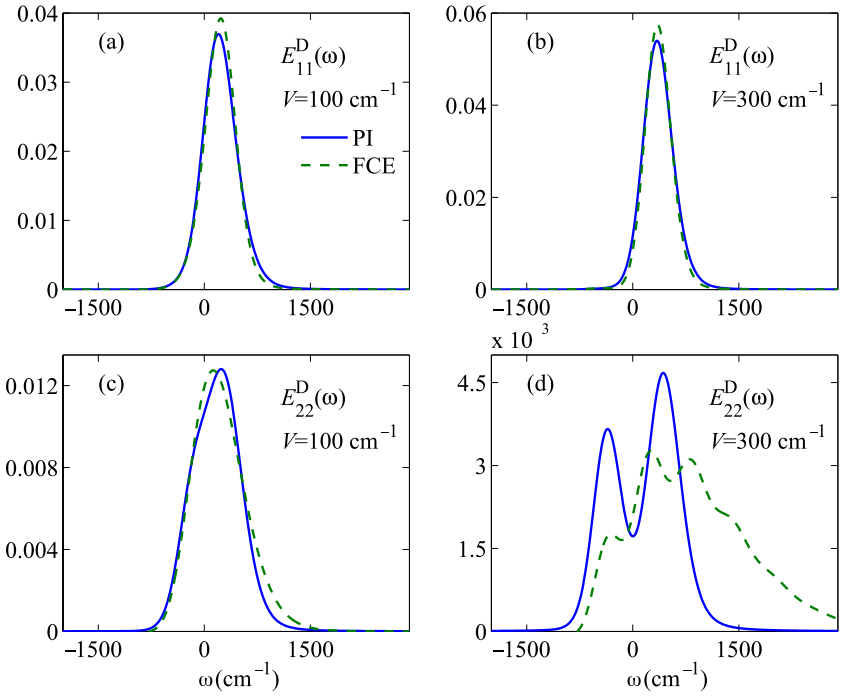

FIG. 7. Comparison of the emission matrix elements obtained by the exact stochastic PI and the FCE methods. The reorganization energy is $\lambda = 200$ cm^{-1}.

a delocalized system, this method can give reliable results only for $\lambda \gg V$. The rate given by the TC2 method is qualitatively tolerant. It is not stable for very large reorganization energy.

Although the emission spectra may not be accurate for delocalized systems, the rate obtained by our cumulant expansion method is still in good agreement with the exact one, since the MCFT rate is proportional to the overlap integral between emission and absorption spectra. If the reorganization energy λ is very large, the height of the spectra is small and the overlap of the spectra is negligible. However, the rate is still problematic for larger real systems, such as LH2, which has motived us to develop the hybrid cumulant expansion and the stochastic path integrals.

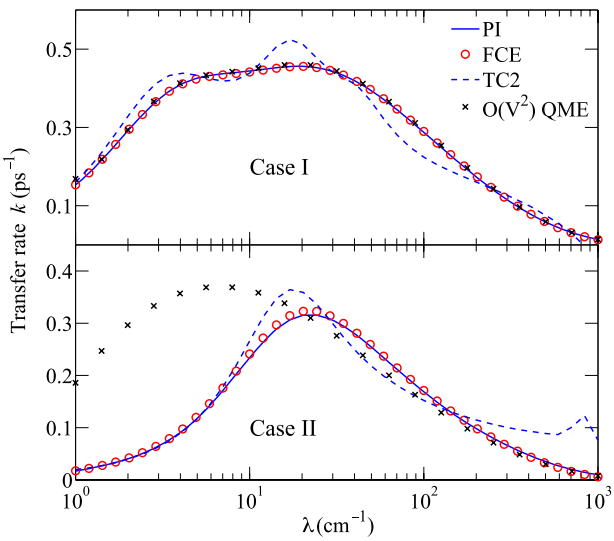

FIG. 8. Comparison of the MCFT rates obtained by the stochastic PI, FCE, TC2[25] and $O(V^2)$ quantum master equation (QME) methods as a function of the reorganization energy λ for the localized (24) and delocalized (25) cases. The bath parameters are the same as in Fig. 2.

V. CONCLUSIONS

In this paper, we study the MCFT rate and the spectra, using a full 2nd-order cumulant expansion, which treats the system-bath interaction Hamiltonian perturbatively, and can reduce to the exact FRET rate for monomers.

(i) For the emission spectrum, the initial state is an equilibrium state of the donor and its bath. Both the donor and the bath deviate from their Boltzmann distributions. Moreover, this equilibrium state cannot be written in a factorized form, and the entanglement between the donor and its bath will affect the subsequent real-time dynamics. The failure of the factorization shows the crucial role of the donor-bath entanglement in both the emission spectrum and the MCFT rate.

(ii) The full cumulant expansion method is applied to both localized and delocalized systems. The absorption spectra obtained by the FCE method are in very good agreement with the exact results for both localized and delocalized cases. Further approximations of the full cumulant expansion can give the inverse participation ratio and the off-diagonal cumulant expansion methods, which overlook the importance of the off-diagonal system-bath coupling and fail to give reliable absorption spectra when the system is delocalized. An alternative solution for absorption spectra was reported during the course of this work.[51]

(iii) The calculation of the emission spectrum is more complicated due to the initial donor-bath entanglement, which depends on the donor-bath interaction and the degree of delocalization. For localized systems, the entanglement is weak, and the full cumulant expansion method performs well. For delocalized systems, the full cumulant expansion method can still give reliable results for low-lying excited states, while the method becomes unreliable for the highly-excited states in the strong system-bath coupling regime. This problem is solved in our Paper II

by combining the cumulant expansion with numerically exact imaginary-time path integrals into a hybrid cumulant expansion.

(iv) In contrast with the emission spectra, the MCFT rate is more robust since it is proportional to the integral overlap between the emission and absorption spectra. The deviations in the spectra are reduced in the transfer rate. Moreover, if the reorganization energy λ is large, the height of the emission spectra is very low and the overlap of the spectra is small. Thus, although the emission spectrum obtained by cumulant expansion may not be reliable in the strong system-bath coupling regime, we can still obtain a reasonable transfer rate. We should note that this analysis is valid for small systems but not for large systems such as LH2. To solve this problem, we developed two new methods: the hybrid cumulant expansion in Paper II and the stochastic path integral in Paper III.

(v) The full cumulant expansion method cannot give reliable emission spectra for delocalized systems when the reorganization energy is large and the thermal energy is small. We develop several new methods to overcome this problem. When the reorganization energy λ is dominant, perturbation can be carried out in the system's off-diagonal coupling V up to 2nd-order.[46] For more complicated systems such as LH2 (see Paper IV), traditional perturbation methods fail to give reliable emission spectra and MCFT rates since the energy gap of the first excitations, the thermal energy, and the reorganization energy are comparable. In our recently developed hybrid cumulant expansion method, we use the imaginary-time path integrals to obtain the exact reduced density matrix of the donor, from which the displacements of the bath operators can be extracted more precisely. This hybrid method can give much more reliable emission spectrum and MCFT rates for systems like LH2. Furthermore, to overcome the problems of the HEOM method in calculating large system and low-temperature conditions, we implement a stochastic path integral method,[29] which gives us the benchmark.

Note added in proof. Computer codes for stochastic simulations of absorption spectra, emission spectra, and Forster rates are available for download at http://web.mit.edu/jianshucaogroup/resources.html.

ACKNOWLEDGMENTS

This work was supported by the National Science Foundation (Grant No. CHE-1112825) and the Defense Advanced Research Planning Agency (Grant No. N99001-10-1-4063). Jian Ma also thanks Liam Cleary and Jeremy Moix for helpful discussions.

APPENDIX: BATH CORRELATION FUNCTION AND LINESHAPE MATRICES

1. Bath correlation function

The general form of the bath correlation function can be derived as

$$C^B(t-i\tau) = \int_0^\infty \frac{d\omega}{\pi} J(\omega) \frac{\cosh\left[\omega\left(\frac{1}{2}\beta - i(t-i\tau)\right)\right]}{\sinh\left[\frac{1}{2}\omega\beta\right]}$$
$$= \frac{4\lambda}{\beta}\left\{\frac{1}{2}e^{-\gamma|t|} + \gamma\sum_{k=1}^{\infty}\frac{\cos(\nu_k\tau)\left(\gamma e^{-\gamma|t|} - \nu_k e^{-\nu_k|t|}\right)}{\gamma^2-\nu_k^2} - i\,\mathrm{sgn}(t)\,\gamma\sum_{k=1}^{\infty}\frac{\sin(\nu_k\tau)\left(\nu_k e^{-\gamma|t|} - \nu_k e^{-\nu_k|t|}\right)}{\gamma^2-\nu_k^2}\right\}, \quad \text{(A1)}$$

where $J(\omega)$ is the Drude spectrum, $\nu_k = 2\pi k/\beta$ is the Matsubara frequency, and $\mathrm{sgn}(x)$ is the sign function.

2. Lineshape matrix K(t)

The matrix $\mathbf{K}(t)$ in Eq. (35) is given by

$$\mathbf{K}(t) = \int_0^t dt_2 \int_0^{t_2} dt_1 \mathrm{tr}_b\left[H_{sb}^A(t_2) H_{sb}^A(t_1)\rho_b^A\right]$$
$$= \sum_{\mu,\nu=1}^{N_A}|\mu\rangle\langle\nu| \sum_{\alpha=1}^{N_A}\sum_{n=1}^{N_A} X_n^{\mu\alpha}X_n^{\alpha\nu}\int_0^t dt_2\int_0^{t_2} dt_1 e^{i\omega_{\mu\alpha}t_2 - i\omega_{\nu\alpha}t_1} C^B(t_2-t_1), \quad \text{(A2)}$$

where the bath correlation function is

$$C^B(t_2-t_1) = \lambda\gamma\left[\cot\left(\frac{\gamma\beta}{2}\right) - i\right]e^{-\gamma|t_2-t_1|} + \frac{4\lambda\gamma}{\beta}\sum_{n=1}^{\infty}\frac{\nu_n e^{-\nu_n|t_2-t_1|}}{\nu_n^2-\gamma^2}.$$

In the high-temperature limit, we can neglect all the Matsubara terms, and thus,

$$C^B(t_2-t_1) = \lambda\gamma\left[\cot\left(\frac{\gamma\beta}{2}\right) - i\right]e^{-\gamma|t_2-t_1|}. \quad \text{(A3)}$$

In this case, the matrix elements can be derived as

$$K_{\mu\nu}(t) = \sum_{\alpha}\sum_{n} X_n^{\mu\alpha} X_n^{\alpha\nu} \int_0^t dt_2 \int_0^{t_2} dt_1 e^{i\omega_{\mu\alpha}t_2 - i\omega_{\nu\alpha}t_1} C(t_2 - t_1)$$
$$= \sum_{\alpha}\sum_{n} X_n^{\mu\alpha} X_n^{\alpha\nu} \lambda_n \gamma \left[\cot\left(\frac{\gamma\beta}{2}\right) - i\right] F_{\mu\alpha\nu}(t),$$

where

$$F_{\mu\alpha\nu}(t) = \frac{e^{-\gamma t + i\omega_{\mu\alpha}t} - 1}{(\gamma - i\omega_{\mu\alpha})(\gamma - i\omega_{\nu\alpha})} + \frac{e^{i\omega_{\mu\nu}t} - 1}{i\omega_{\mu\nu}(\gamma - i\omega_{\nu\alpha})}. \tag{A4}$$

If $\mu = \nu$, we have

$$F_{\mu\mu\mu} = \frac{e^{-\gamma t} - 1}{\gamma^2} + \frac{t}{\gamma}. \tag{A5}$$

3. Lineshape matrix $\mathbf{K}^{II}(\beta)$

The matrix $\mathbf{K}^{II}(\beta)$ in Eq. (47) is

$$\mathbf{K}^{II}(\beta) = \int_0^\beta d\tau_2 \int_0^{\tau_2} d\tau_1 \mathrm{tr}_b \left[H_{sb}^D(-i\tau_2)\, H_{sb}^D(-i\tau_1)\, \rho_b^D\right]$$
$$= \sum_{\mu\nu\alpha}\sum_{n} X_n^{\mu\alpha} X_n^{\alpha\nu} |\mu\rangle\langle\nu| \int_0^\beta d\tau' e^{\omega_{\mu\nu}\tau'} \int_0^{\tau'} d\tau\, e^{\omega_{\nu\alpha}\tau} C^B(-i\tau),$$

where the imaginary-time correlation function is

$$C^B(-i\tau) = \frac{2\lambda}{\beta} + \frac{4}{\beta}\sum_{k=1}^{\infty} \frac{\lambda\gamma}{\gamma + \nu_k} \cos(\nu_k \tau). \tag{A6}$$

Substituting the above result into $\mathbf{K}^{II}$, we can solve the integral

$$\int_0^{\tau'} d\tau\, e^{\omega_{\nu\alpha}\tau} C^B(-i\tau) = \frac{2\lambda}{\beta} \mathcal{F}_{\nu\alpha}, \tag{A7}$$

where

$$\begin{aligned} \mathcal{F}_{\nu\nu} &= \tau' + 2\gamma \sum_{k=1}^{\infty} \frac{1}{\gamma + \nu_k} \frac{\sin(\nu_k \tau')}{\nu_k}, \\ \mathcal{F}_{\nu\alpha} &= \frac{e^{\omega_{\nu\alpha}\tau'} - 1}{\omega_{\nu\alpha}} + 2\gamma \sum_{k=1}^{\infty} \frac{e^{\omega_{\nu\alpha}\tau'}[\nu_k \sin(\nu_k \tau') + \omega_{\nu\alpha}\cos(\nu_k \tau')] - \omega_{\nu\alpha}}{(\gamma + \nu_k)(\nu_k^2 + \omega_{\nu\alpha}^2)}. \end{aligned} \tag{A8}$$

4. Lineshape matrix $\mathbf{K}^{RR}(t, \beta)$

The matrix $\mathbf{K}^{RR}(t, \beta)$ in Eq. (49) is

$$\mathbf{K}^{RR}(t, \beta) = \int_0^t ds_2 \int_0^{s_2} ds_1 \mathrm{tr}_b \left[H_{sb}^D(s_2 - i\beta)\, H_{sb}^D(s_1 - i\beta)\, \rho_b^D\right]$$
$$= \sum_{\mu\nu\alpha}\sum_{n} X_n^{\mu\alpha} X_n^{\alpha\nu} |\mu\rangle\langle\nu| e^{\beta\omega_{\mu\nu}} \int_0^t ds_2\, e^{i\omega_{\mu\nu}s_2} \int_0^{s_2} ds_1\, e^{i\omega_{\nu\alpha}s_1} C^B(s_1),$$

where

$$C^B(s) \simeq \lambda\gamma \left[\cot\left(\frac{\gamma\beta}{2}\right) - i\right] e^{-\gamma s}. \tag{A9}$$

5. Lineshape matrix $\mathbf{K}^{RI}(t,\beta)$

The matrix $\mathbf{K}^{RI}(t,\beta)$ in Eq. (50) is

$$\begin{aligned}\mathbf{K}^{RI}(t,\beta) &= \int_0^t ds \int_0^\beta d\tau \mathrm{tr}_b \left[H_{sb}^D(s-i\beta)\, H_{sb}^D(-i\tau)\, \rho_b^D\right] \\ &= \sum_{\mu\nu\alpha}\sum_n X_n^{\mu\alpha} X_n^{\alpha\nu} |\mu\rangle\langle\nu| e^{\beta\omega_{\mu\alpha}} \int_0^t ds \int_0^\beta d\tau e^{i\omega_{\mu\alpha}s - \omega_{\nu\alpha}\tau} C^B(-s-i\tau)\,,\end{aligned}$$

where

$$\begin{aligned}C^B(-s-i\tau) = \frac{4\lambda}{\beta}\Bigg\{\frac{1}{2}e^{-\gamma s} &+ \gamma\sum_{k=1}^{\infty}\frac{\cos(\nu_k\tau)\left(\gamma e^{-\gamma s} - \nu_k e^{-\nu_k s}\right)}{\gamma^2-\nu_k^2} \\ &+ i\gamma\sum_{k=1}^{\infty}\frac{\sin(\nu_k\tau)\left(\nu_k e^{-\gamma s} - \nu_k e^{-\nu_k s}\right)}{\gamma^2-\nu_k^2}\Bigg\}. \qquad \text{(A10)}\end{aligned}$$

[1]V. M. Agranovich and M. D. Galanin, *Electronic Excitation Energy Transfer in Condensed Matter*, 3rd ed. (North-Holland Publishing Company, Amsterdam, 1982).
[2]D. L. Andrews and A. A. Demidov, *Resonance Energy Transfer* (John Wiley and Sons, Chichester, 1999).
[3]V. May and O. Kühn, *Charge and Energy Transfer Dynamics in Molecular Systems* (Wiley-VCH, Weinheim, 2004).
[4]T. Förster, in *Modern Quantum Chemistry*, edited by O. Sinanoglu (Academic Press, New York, 1965), Vol. 3.
[5]H. Sumi, J. Phys. Chem. B **103**, 252 (1999).
[6]R. E. Blankenship, *Molecular Mechanisms of Photosynthesis* (Blackwell Science, London, 2002).
[7]T. Renger, V. May, and O. Kühn, Phys. Rep. **343**, 137 (2001).
[8]V. I. Novoderezhkin and R. van Grondelle, Phys. Chem. Chem. Phys. **12**, 7352 (2010).
[9]M. A. Bopp, A. Sytnik, T. D. Howard, R. J. Cogdell, and R. M. Hochstrasser, Proc. Natl. Acad. Sci. U.S.A. **96**, 11271 (1999).
[10]A. M. van Oijen, M. Ketelaars, J. Köhler, T. J. Aartsma, and J. Schmidt, Science **285**, 400 (1999).
[11]L. Cleary, H. Chen, C. Chuang, R. J. Silbey, and J. Cao, Proc. Natl. Acad. Sci. U.S.A. **110**, 8537 (2013).
[12]J. Ye, K. Sun, Y. Zhao, Y. Yu, C. K. Lee, and J. Cao, J. Chem. Phys. **136**, 245104 (2012).
[13]G. S. Engel, T. R. Calhoun, E. L. Read, T.-K. Ahn, T. Mančal, Y.-C. Cheng, R. E. Blankenship, and G. R. Fleming, Nature **446**, 782 (2007).
[14]I. P. Mercer, Y. C. El-Taha, N. Kajumba, J. P. Marangos, J. W. G. Tisch, M. Gabrielsen, R. J. Cogdell, E. Springate, and E. Turcu, Phys. Rev. Lett. **102**, 057402 (2009).
[15]E. Collini, C. Y. Wong, K. E. Wilk, P. M. G. Curmi, P. Brumer, and G. D. Scholes, Nature **463**, 644 (2010).
[16]H. Lee, Y.-C. Cheng, and G. R. Fleming, Science **316**, 1462 (2007).
[17]D. Abramavicius, B. Palmieri, D. V. Voronine, F. Šanda, and S. Mukamel, Chem. Rev. **109**, 2350 (2009).
[18]M. Cho, Chem. Rev. **108**, 1331 (2008).
[19]D. M. Jonas, Science **300**, 1515 (2003).
[20]J. L. Herek, N. J. Fraser, T. Pullerits, P. Martinsson, T. Polivka, H. Scheer, R. J. Cogdell, and V. Sundstrom, Biophys. J. **78**, 2590 (2000).
[21]X. Hu, T. Ritz, A. Damjanovic, F. Autenrieth, and K. Schulten, Q. Rev. Biophys. **35**, 1 (2002).
[22]D. Beljonne, C. Curutchet, G. D. Scholes, and R. J. Silbey, J. Phys. Chem. B **113**, 6583 (2009).
[23]L. Cleary and J. Cao, New J. Phys. **15**, 125030 (2013).
[24]G. D. Scholes, Annu. Rev. Phys. Chem. **54**, 57 (2003).
[25]S. Jang, M. D. Newton, and R. J. Silbey, Phys. Rev. Lett. **92**, 218301 (2004).
[26]J. Wu and J. Cao, J. Chem. Phys. **139**, 044102 (2013).
[27]B. Mennucci and C. Curutchet, Phys. Chem. Chem. Phys. **13**, 11538 (2011).
[28]S. Mukamel, *Principles of Nonlinear Optical Spectroscopy* (Oxford University Press, 1995).
[29]J. Moix, J. Ma, and J. Cao, "Förster resonance energy transfer, absorption and emission spectra in multichromophoric systems. III. Exact stochastic path integral evaluation," J. Chem. Phys. **142**, 094108 (2015).
[30]A. Ishizaki and G. R. Fleming, J. Chem. Phys. **130**, 234111 (2009).
[31]L. Chen, R. Zheng, Q. Shi, and Y. Yan, J. Chem. Phys. **131**, 094502 (2009).
[32]J. Strümpfer and K. Schulten, J. Chem. Phys. **134**, 095102 (2011).
[33]Y. Jing, L. Chen, S. Bai, and Q. Shi, J. Chem. Phys. **138**, 045101 (2013).
[34]T. Renger and R. A. Marcus, J. Chem. Phys. **116**, 9997 (2002).
[35]L. Banchi, G. Costagliola, A. Ishizaki, and P. Giorda, J. Chem. Phys. **138**, 184107 (2013).
[36]S. Maier, T. L. Schmidt, and A. Komnik, Phys. Rev. B **83**, 085401 (2011).
[37]C. K. Lee, J. Moix, and J. Cao, J. Chem. Phys. **136**, 204120 (2012).
[38]M. Yang, J. Chem. Phys. **123**, 124705 (2005).
[39]W. M. Zhang, T. Meier, V. Chernyak, and S. Mukamel, J. Chem. Phys. **108**, 7763 (1998).
[40]V. I. Novoderezhkin, M. A. Palacios, H. van Amerongen, and R. van Grondelle, J. Phys. Chem. B **108**, 10363 (2004).
[41]M. Cho, H. M. Vaswani, T. Brixner, J. Stenger, and G. R. Fleming, J. Phys. Chem. B **109**, 10542 (2005).
[42]M. Yang and G. R. Fleming, Chem. Phys. **282**, 163 (2002).
[43]K. Ohta, M. Yang, and G. R. Fleming, J. Chem. Phys. **115**, 7609 (2001).
[44]M. Schröder, U. Kleinekathöfer, and M. Schreiber, J. Chem. Phys. **124**, 084903 (2006).
[45]S. Yang, J. Shao, and J. Cao, J. Chem. Phys. **121**, 11250 (2004).
[46]L. Cleary and J. Cao, "Multichromophoric Förster resonance energy transfer via a weak intracomplex coupling quantum master equation" (unpublished).
[47]J. Ma, J. Moix, and J. Cao, "Förster resonance energy transfer, absorption and emission spectra in multichromophoric systems. II. Hybrid cumulant expansion," J. Chem. Phys. **142**, 094107 (2015).
[48]J. Moix, J. Ma, and J. Cao, "Exact evaluation of the energy transfer rates and steady state absorption and emission spectra in the b850 photosynthetic complexes of LH2" (unpublished).
[49]J. Wu, F. Liu, Y. Shen, and J. Cao, New J. Phys. **12**, 105012 (2010).
[50]J. Moix, Y. Zhao, and J. Cao, Phys. Rev. B **85**, 115412 (2012).
[51]T. Dinh and T. Renger, J. Chem. Phys. **142**, 034104 (2015).